JOURNAL OF Materials CHEMISTRY

How to tailor maghemite particle size in γ-Fe_2O_3–SiO_2 nanocomposites

C. Cannas,[a] G. Concas,[c] D. Gatteschi,[b] A. Musinu,[a] G. Piccaluga[a] and C. Sangregorio[b]

[a]*Dipartimento di Scienze Chimiche, Cittadella Universitaria di Monserrato, I-09042, CA, Italy*
[b]*Dipartimento di Chimica, Università di Firenze, INSTM, I-50019 SestoFiorentino, FI, Italy*
[c]*Dipartimento di Fisica, Università di Cagliari e INFM, Cittadella Universitaria di Monserrato, I-09042, CA, Italy*

Received 3rd May 2002, Accepted 5th July 2002
First published as an Advance Article on the web 13th August 2002

A sol–gel procedure for the tailoring of maghemite particle size in silica-based nanocomposites is proposed. The preparation method allows control of the gelation time, which is varied from 2 to 16 days in samples having the same concentration of iron oxide (25%). Superparamagnetic particles of γ-Fe_2O_3 with sizes in the 2.5–5.6 nm range were found in all the samples, as confirmed by TEM, Mössbauer spectroscopy and magnetic measurements. The particle size was independent of the porosity of the silica host matrix, but strongly dependent on the amount of solvent trapped inside the gels. The solvent plays an important role, favouring the formation of Fe_3O_4 nanoparticles as an intermediate step before the final oxidation to maghemite.

Introduction

New processes for preparing nanosized γ-Fe_2O_3 (maghemite) particles are of particular interest for various technological applications, mainly because of their peculiar magnetic properties. Maghemite nanoparticles are ferrimagnetic and characterised by the superparamagnetic relaxation phenomenon, which is strongly affected by particle size, shape and by various surface effects. The interesting magnetic properties of nanostructured maghemite are due to finite size effects and/or high surface/volume ratios, thus making the study of the interrelation between microstructure and magnetism very appealing. Recently, several preparation methods, *e.g.* thermal decomposition of lepidocrocite,[1] co-precipitation from solution and laser pyrolysis,[2] microwave plasma,[3] electrochemical synthesis[4] and mechanical activation,[5] have been developed, aimed at tailoring the particle size of pure maghemite. To create an obstacle towards particle aggregation, the preparation of maghemite dispersed over inert matrices has been attempted. Achieving particle size control in these nanocomposites is certainly more difficult. Therefore, most of the work[6–19] is devoted to a careful investigation of the relationship between particle size and magnetic properties rather than searching for the appropriate preparation conditions which favour the particle size control.

Among the various preparation methods, we experimented with the sol–gel route, which was found to be effective for achieving γ-Fe_2O_3–SiO_2 nanocomposites. In the first adopted method, which starts from mixtures of tetraethyl orthosilicate (TEOS) and hydroethanolic solutions of iron nitrate,[14,15] iron oxide nanoparticles homogeneously dispersed in the silica matrix were obtained, but some difficulties were encountered in achieving systems containing only the maghemite phase. In fact, for high iron oxide contents, antiferromagnetic α-Fe_2O_3 nanoparticles were also formed.[14,15] The outcomes of the preparation were later improved by changing the process parameters of the sol–gel technique, using ethylene glycol as the starting solvent, but small traces of the antiferromagnetic phases were still present in the final samples.[16] Some authors report the evolution from the γ- to the α-Fe_2O_3 phases as a size-dependent transition:[20] a decrease in particle size seems to provide better stability of γ-Fe_2O_3. According to this point of view, it is necessary to carefully control the size of the particles at all the stages of the preparation in order to achieve samples where only the maghemite phase is formed. The kind of oxide phase obtained in the final nanocomposites is also strongly affected by the nanoparticle precursor formed at the first stage of preparation and thermal treatment. In our samples, poorly crystallised particles of the *2l*-ferrihydrite phase were recognised as precursors of iron oxide particles.[21] Similar results were obtained by Niznaski *et al.*,[11] while the formation of magnetite (Fe_3O_4) was hypothesised to be the determinant step in the sol–gel preparation of γ-Fe_2O_3–SiO_2 nanocomposites by Del Monte *et al.*[13] This result was ascribed to a reduction reaction promoted by the residual organic solvent still present in the gel. An analogous mechanism might be responsible for the not well understood presence of ferrous iron found in appreciable amounts in the product of a sol–gel reaction, and which, after thermal treatment, yielded the maghemite phase.[9] Moreover, the preparation of bulk maghemite through oxidation of magnetite is, at present, the most commonly used method.[22] In the light of these observations, a slight variation of the gelation conditions previously used in our procedure was introduced, which favours the trapping of the organic solvent in the gel. In this way, nanocomposites containing only the maghemite phase were obtained.[23]

In order to explore the utility of this sol–gel procedure for the tailoring of maghemite particle size, a novel approach which allows the control of gelation time was tested. To this end, a series of Fe_2O_3–SiO_2 nanocomposites were prepared, each having the same composition (25 wt% of iron oxide) but obtained with gelation times in the range 2–16 days and then submitted to thermal treatment in oxidising or inert atmospheres. This work may acheive another goal. In fact, this procedure, if the thermal treatment of the gel is carried out in an inert atmosphere, might unambiguously demonstrate whether the Fe_3O_4 phase forms as a precursor. The structure of the samples was characterised by X-ray diffraction (XRD), transmission electron microscopy (TEM) and Mossbauer spectroscopy. Magnetic properties were also checked through magnetisation measurements recorded at low temperature.

DOI: 10.1039/b204292d

Since the porous structure of the silica may have a great influence on the formation of maghemite nanoparticles, the textural properties were investigated through N_2 physisorption measurements.

Experimental

The starting sol was obtained by mixing TEOS (Aldrich, 98%) and an ethanolic solution (Ethanol, Carlo Erba, 99%) of iron nitrate nonahydrate [$Fe(NO_3)_3 \cdot 9H_2O$, Aldrich, 98%] with a TEOS : EtOH : water molar ratio of 0.46 : 2 : 1, following the procedure reported in ref. 23. The hydrolysis reaction was promoted only by the hydration water of the salt. The sol, with an initial pH of about 1, was stirred for 15 min and then poured into five separate identical vessels. Each vessel contained different volumes of the sol, therefore determining a variation in the surface/volume (S/V) ratio. The vessels were closed using a seal with a small punched hole and then heated in an oven at 50 °C up to the gel point. The gelation time for the nanocomposites varied between 2 to 16 days, depending on the S/V ratio. The parameters of the preparation are reported in Table 1, together with the acronyms used below. The fresh monolithic gels were directly calcined at 400 °C in static air for 4 h and then powdered. Some portions of the A and D gels were calcined at 400 °C in flowing nitrogen (reported in the following as samples A_1 and D_1, and then treated in static air for 4 h at 400 °C.

XRD powder patterns were collected between 4 and 36° 2Θ using a Siemens D500 diffractometer with Mo-Kα radiation. TEM analysis was performed with a JEOL 200CX microscope operating at 200 kV.

Mössbauer absorption spectra of samples A, C and D were obtained in standard transmission geometry, using a source of ^{57}Co in rhodium (370 MBq). Calibration was performed using a 25 μm thick natural iron foil; the isomer shift values are referred to α-Fe. The measurements were performed using a flow cryostat with mylar windows; helium was used as the cryogenic liquid. These measurements were carried out using a copper sample holder maintained in exchange gas (helium); the powders were kept between two layers of Plexiglas. The surface density of the absorber was 70, 120 and 180 mg cm^{-2} for the samples A, C and D, respectively.

Measurements of magnetic susceptibility of the three samples were performed on a Cryogenics S600X SQUID magnetometer equipped with a superconducting magnet producing fields up to 70 kOe. Zero field cooled (ZFC) susceptibilities were measured by cooling samples in zero magnetic field and then by increasing the temperature in an applied field of 50 Oe, while field cooled (FC) curves were recorded by cooling the samples in the same field of 50 Oe.

N_2 physisorption measurements were performed on a Sorpomatic 1990 system (Fisons Instruments) by determining the N_2 adsorption–desorption isotherms at 77 K. Before analysis, the samples were outgassed at 200 °C for 18 h. The surface area (S_{BET}) was estimated by the Dubinin–Raduskevitch method.

Table 1 Preparation conditions for the sol–gel samples ($Fe_2O_3/Fe_2O_3 + SiO_2 = 25$ wt%)

Sample	Sol volume/ml	S/V ratio/mm^{-1}	Gelation time/days
A	20	0.04	16
B	15	0.05	12
C	7.5	0.1	8
D	2.5	0.30	3.5
E	1.75	0.40	2

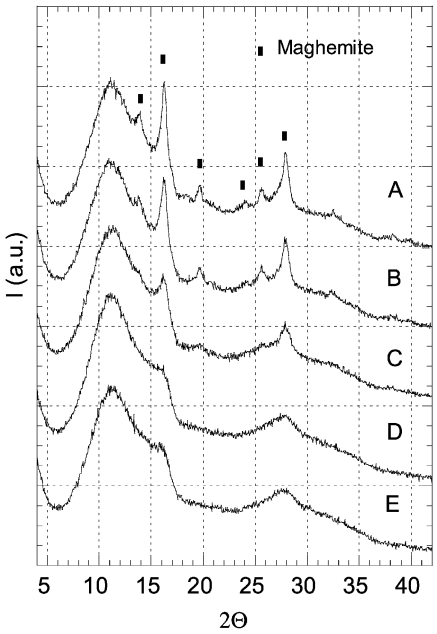

Fig. 1 XRD spectra of the nanocomposites calcined in air.

Results and discussion

XRD spectra of all the samples calcined in air at 400 °C are presented in Fig. 1. All the spectra show a broad halo due to amorphous silica, with a series of crystalline peaks, which are due to the iron oxide phase formed. In particular, the spectrum of sample A exhibits a series of diffraction peaks which, on the basis of their position and relative intensity, unequivocally indicate that the formed phase is γ-Fe_2O_3. These peaks become progressively broader in the spectra of the other samples (from A to E), up to the disappearance of the less intense peaks in the spectra of samples D and E. The indication of a unique phase is supported by the regular evolution of all the spectra. The observed trend suggests a possible decrease in the particle size with gelation time, which is consistent with the particle size distribution obtained by TEM analysis reported below, but a careful identification of the iron oxide phase has to be made before any further analysis. In fact, in the spectra of samples D and E only two broad peaks remain, falling at positions consistent with the *d*-spacing typical of several iron oxides, hydroxide or oxyhydroxide, including the phase known as *2l*-ferrihydrite found in our previous samples.[21] Therefore, on the basis of XRD results only, an unequivocal identification of the iron oxide phase is not possible for the most disordered samples, and corroboration from other structural or magnetic techniques is required.

The Mössbauer absorption spectra of samples A, C and D, recorded at 4.2 K, are shown in Fig. 2. All the spectra show a sextet due to the magnetic blocked state of the particles and have been analyzed with Lorentzian-shaped peaks, using a least squares method. The results of the fitting are given in Table 2, where the isomer shift (δ), full width at half maximum (Γ) and hyperfine internal magnetic field (B) values are reported. The broadening of the Zeeman split lines is an effect of the size distribution of the particles; particles with different volume have a different magnetic field because of the effect of the collective magnetic excitations.[24,25] As regards the iron oxide phase formed, the Mössbauer investigation clearly indicates that the same phase forms in all the samples and that this phase is maghemite. The indication of a unique phase is strongly supported by the regular evolution of all the spectral parameters (consistent with the trend in the XRD spectra), which do not suggest a discontinuity in the type of phase formed. Moreover, the values obtained for the magnetic field,

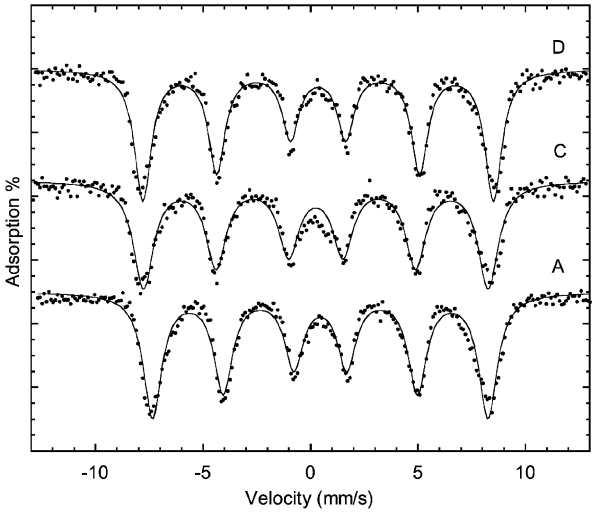

Fig. 2 Mössbauer spectra of the A, C and D nanocomposites at 4.2 K. The experimental points (dots) and the calculated data (solid line) are shown.

Table 2 Mössbauer parameters obtained by fitting the spectra of nanocomposites A, C and D collected at 4.2 K. The table shows the isomer shift (δ), full width at half maximum of the peaks (Γ) and magnetic field (B) values. Statistical errors are given in parentheses

Sample	δ/mm s^{-1}	Γ/mm s^{-1}	B/T
A	0.47(1)	0.94(2)	51.0(1)
C	0.46(1)	1.13(2)	50.2(1)
D	0.47(1)	1.04(1)	48.9(1)

which range from 48.9 (sample D) to 51.0 T (sample A), are typical of the values reported for nanocrystalline maghemite at 4 K (49–52 T, depending on the particle size),[26] and smaller than the value for the bulk maghemite (52.6 T).[26] It is important to note that the *2l*-ferrihydrite presents smaller magnetic field values (48 T).[27]

The temperature dependence of the ZFC and FC static susceptibilities for samples A, C and D are shown in Fig. 3. The FC and ZFC curves coincide at high temperature for all the samples and the susceptibility follows a Curie–Weiss law at a first approximation. They begin to separate as the temperature decreases and the ZFC curves exhibit maxima. Such behaviour is characteristic of superparamagnetism[25–28] and is due to the progressive deblocking of particles of increasing size as the temperature rises. It is generally assumed that the temperature of the maximum (T_{max}) depends on the average particle size, while the temperature at which the FC and ZFC curves start to separate (T_{sep}) corresponds to the blocking of the largest particles. The difference between T_{sep} and T_{max} therefore represents a qualitative measure of the nanoparticle size distribution. The almost coincident values of T_{sep} and T_{max} evidence a narrow size distribution in all the samples, while the increase of T_{max} (35, 70, 180 K) from sample D to A indicates that the average particle size increases, in agreement with the trend observed in the XRD data and confirmed by the TEM analysis reported below.

Below T_{max}, hysteretic behaviour is observed, as shown in Fig. 4, where the hysteresis loops of samples A, C and D recorded at 2.5 K are reported. The curves display the typical features of randomly oriented assemblies of nanosized single domain particles. All samples exhibit magnetisation values which are far from saturation up to the highest measuring field (6.5 T). The saturation values extrapolated from the high field parts of the curves are lower than that of bulk maghemite (82 emu g^{-1}) and in good agreement with values previously observed for maghemite particles of comparable size.[2,4,14,23]

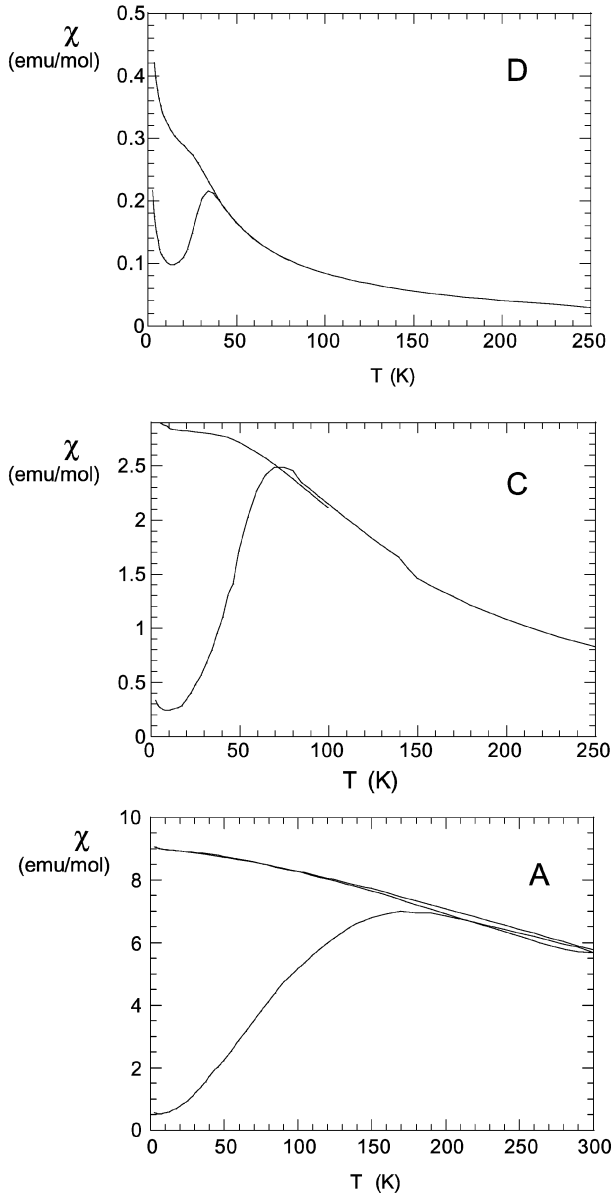

Fig. 3 ZFC (lower curves) and FC (upper curves) magnetisations measured as a function of temperature for nanocomposites A, C and D.

The reduced remanence decreases with particle size from 0.22 (sample A) to 0.13 (sample C) and is extremely small for sample D (0.04), which may contain a not negligible amount of a paramagnetic impurity, as also suggested by the low temperature paramagnetic behaviour observed in the ZFC–FC curve. The largest coercive field is observed for sample A, 132 mT, while sample A and D have similar values, 82 and 80 mT, respectively.

The quantitative estimation of maghemite particle sizes and their distribution has been made *via* TEM analysis. TEM bright field micrographs (Fig. 5) evidence differences in the morphology of the samples, showing a very homogeneous dispersion of isolated nanoparticles over silica in sample D, while nanoparticles located in large and irregular aggregates (in the range 20–200 nm) within the amorphous silica network are revealed starting from sample C. Three dark field images for samples A, C and D are presented in Fig. 6; they show the presence of iron oxide nanoparticles dispersed over the amorphous silica matrix. The size distributions are reported in Fig. 7. The mean particle size decreases regularly from sample A to D, confirming that the peak broadening observed in the

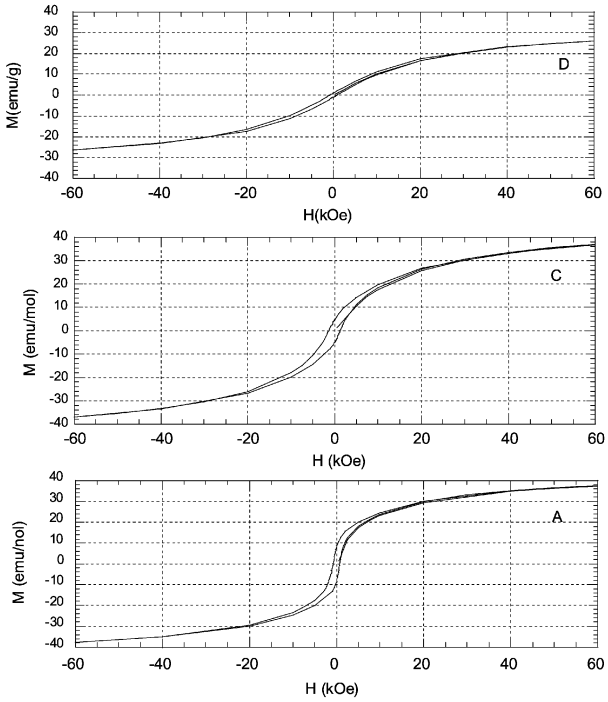

Fig. 4 Magnetic hysteresis loops of nanocomposites A, C and D measured at 2.5 K.

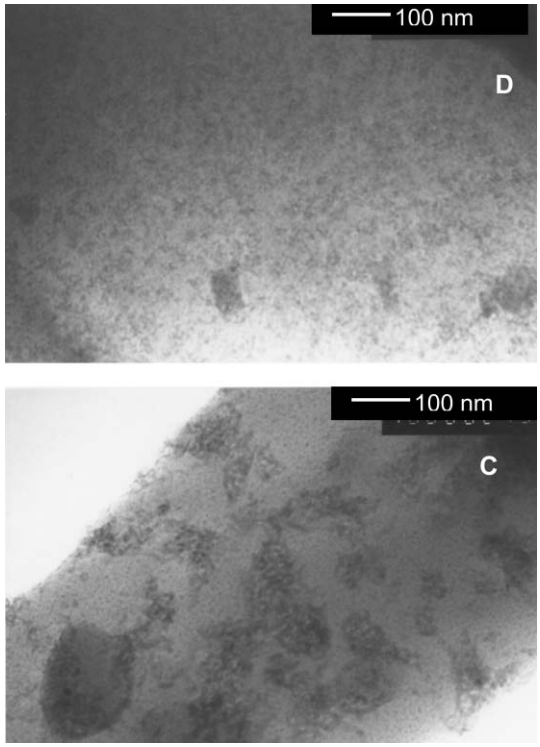

Fig. 5 TEM bright field micrographs of nanocomposites C and D.

XRD spectra is due to the reduction in maghemite particle size, while the size distribution becomes narrower, in agreement with the susceptibility curves.

Therefore, a correlation between the mean particle size and gelation time exists, thus indicating that the particle size can be successfully controlled by choosing the S/V conditions (Table 1), which determine the appropriate gelation time.

In order to understand whether these findings might be correlated with different textural properties of the matrix,

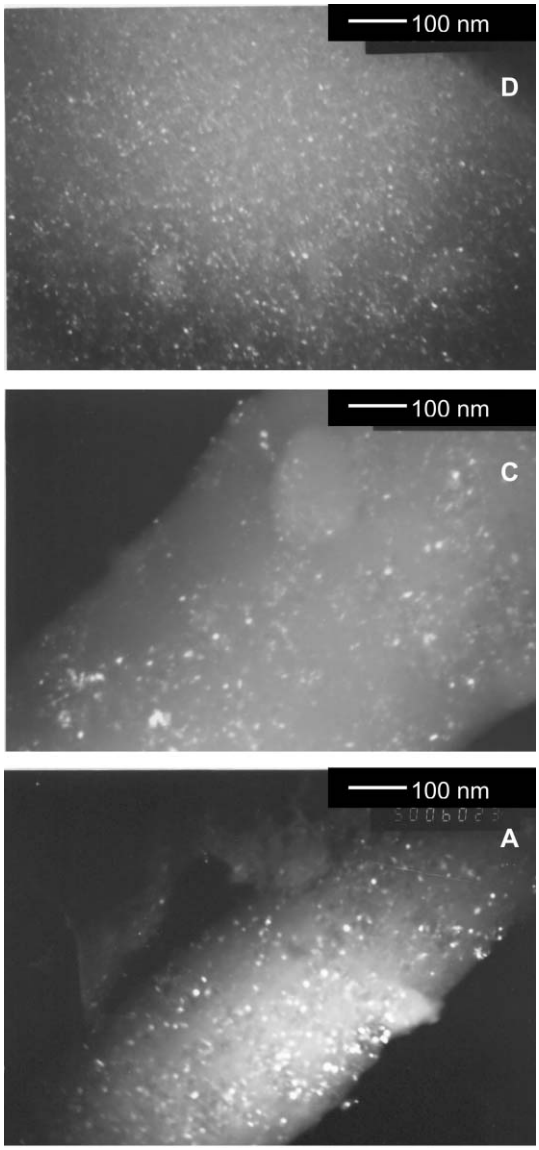

Fig. 6 TEM dark field micrographs of nanocomposites A, C and D.

inferred by the gelation conditions, N_2 physisorption results were collected for the nanocomposites and pure silica samples obtained under the same experimental conditions, and are summarised in Table 3. The pore size distribution was estimated by the Kawazoe–Howorth method.[29] On the whole, all the samples present a microporous structure, which cannot account for the accommodation of particles having a size larger than the pore itself. This is certainly true for micropores (<20 Å); but the amount of mesopores (sizes in the range 20–500 Å) is also very low and discontinuous going from sample A to E. In contrast, by increasing the gelation time, the surface area increases both in the nanocomposites and the pure silica samples. This trend is less evident for the nanocomposites, being an obvious consequence of partial surface coating by nanoparticles. Therefore, the different particle size is independent of the porosity, while a larger surface area might be responsible for the coalescence and growth of particles which, reasonably, are not encapsulated inside narrow cavities. NiO particles larger than the average pore sizes were also found in silica-based nanocomposites prepared by sol–gel methods.[30] In this respect, long gelation times allow this process to became easier, though a less homogeneous dispersion is also obtained, according to the TEM micrographs.

The amount of solvent trapped inside the gel also plays an important role. The weighed amount of final gel is reduced to

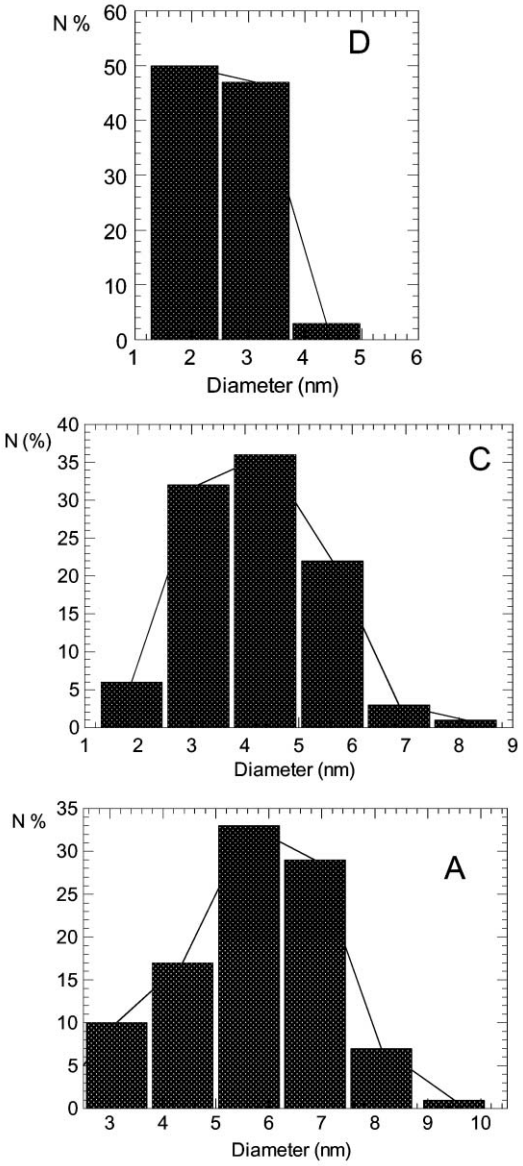

Fig. 7 Particle size distribution for nanocomposites A, C and D.

one half with respect to the starting sol in sample A, while it drops to one quarter in sample E. The high amount of solvent in the samples with long t_{gel} makes moving and coalescence of particle precursors easier. This observation is confirmed by XRD spectra of the gels, shown in Fig. 8, where more intense peaks, ascribed to the presence of iron nitrate, are visible in the

Table 3 Total surface area (S_{BET}) and pore size distribution for all nanocomposites and corresponding silica samples treated at 400 °C

		Pore size distribution/vol%	
	$S_{BET}/m^2\ g^{-1}$	Micropores	Mesopores
Nanocomposites			
A	492	90	10
B	471	95	5
C	445	98	2
D	409	87	13
E	388	89	10
Pure silica samples			
A	674	98	2
B	659	98	2
C	604	99	1
D	490	92	8
E	373	87	13

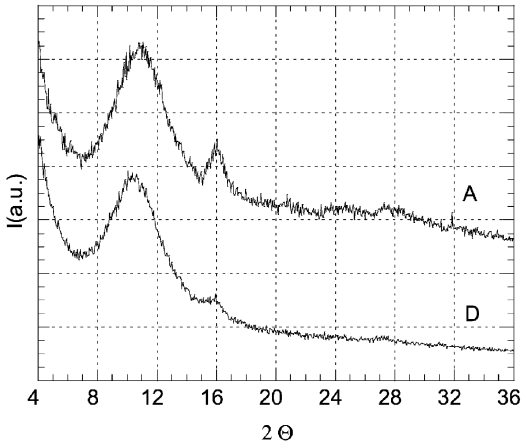

Fig. 8 XRD spectra of gel samples A and D.

A gel compared to the D gel. The solvent content may also be important in another respect. In fact, as reported in the Introduction, the organic residual from the solvent might favour the formation of Fe_3O_4 nanoparticles, which are thought to be the intermediate step before the final oxidation to maghemite. However, structural evidence for this is still lacking.

XRD spectra of the A_1 and D_1 nanocomposites obtained in N_2 at 400 °C are reported in Fig. 9. On the whole, the spectra are very similar to those of the A and D nanocomposites reported in Fig. 1. A series of crystalline peaks, superimposed on that of the silica matrix, fall at *d*-spacing values typical of the Fe_3O_4 phase. In fact, the *d*-spacings of this phase are very close to that of γ-Fe_2O_3, aside from a slight shift toward lower angles, as found in the spectrum of sample A_1. The cell constant calculated for sample A_1 (8.38 Å) corresponds, within the limits of the experimental error, to that of Fe_3O_4, (PDF card no. 19-0629), while a lower value is obtained from the XRD spectrum of sample A (8.323 Å), which corresponds to the cell constant of maghemite (PDF card no. 39-1346). Moreover, the characteristic black color of samples A_1 and D_1 is consistent with the presence of Fe_3O_4. The same trend as found for the samples treated in air is observed in the spectra of the samples treated in nitrogen, in terms of peak broadening as a function of gelation time. The slight shift of the two large peaks in the spectrum of sample D_1 with respect to sample D also confirms the identification of the Fe_3O_4 phase. After treatment in air at 400 °C, the XRD spectra of samples A_1 and D_1 become identical to those of samples A and D, confirming the formation of maghemite nanoparticles through oxidation of magnetite. Therefore, under an inert atmosphere, the solvent organic residuals act as a reductant, leading to the

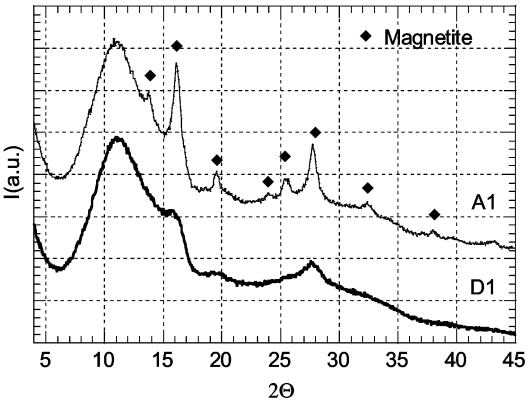

Fig. 9 XRD spectra of the A1 and D1 nanocomposites calcined in flowing nitrogen at 400 °C.

formation of magnetite; this process is not apparent if completely carried out in air because subsequent oxidation of magnetite to maghemite is almost instantaneous.

Conclusion

A sol–gel procedure which allows control of the gelation time has proved successful for the tailoring of maghemite particle size in silica-based nanocomposites. The gelation time was varied between 2 to 16 days, with all samples having an iron oxide concentration of 25%. Superparamagnetic particles of γ-Fe_2O_3 were found in all the samples with sizes in the 2.5–5.6 nm range, as confirmed by TEM, Mössbauer spectroscopy and magnetic measurements. The particle size is not affected by the porosity of silica host matrix, but strongly dependent on the amount of solvent trapped inside the gels. The solvent plays an important role, favouring the formation of Fe_3O_4 nanoparticles as an intermediate step before the final oxidation to maghemite.

Acknowledgement

The financial support of MIUR, CNR PF MSTA is gratefully acknowledged.

References

1 G. S. Chopra, G. Real, M. D. Acalà, L. A. Perez-Maqueda, J. Subrt and J. M. Criado, *Chem. Mater.*, 1999, **11**, 1128.
2 M. P. Morales, S. Veintemillas-Verdaguer, M. I. Montero, C. J. Serna, A. Roig, L. I. Casas, B. Martinez and F. Sandiumenge, *Chem. Mater.*, 1999, **11**, 3058.
3 D. Vollath, D. Szabò, R. D. Taylor and J. O. Willis, *J. Mater. Res.*, 1997, **12**, 2175.
4 C. Pascal, J. L. Pascal, F. Favier, M. L. Elidrissi Moubtassim and C. Payen, *Chem. Mater.*, 1999, **11**, 141.
5 J. Xue, Z. Zhou and J. Wang, *J. Am. Ceram. Soc.*, 2002, **85**(4), 807.
6 T. Ida, H. Tsuiki, A. Ueno, K. Tohji, Y. Udagawa, K. Iwai and H. Sano, *J. Catal.*, 1987, **106**, 428.
7 R. F. Ziolo, E. P. Giannelis, B. A. Weinstein, M. P. O'Horo, B. N. Ganguly, V. Mehrotra, M. W. Russel and D. Huffman, *Science*, 1992, **257**, 219.
8 J. P. Wang and H. L. Luo, *J. Magn. Magn. Mater.*, 1994, **131**, 54.
9 G. M. da Costa, E. De Grave, P. M. A. de Bakker and R. E. Vandenberghe, *J. Solid State Chem.*, 1994, **113**, 405.
10 L. Zhang, G. C. Papaefthymiou, R. F. Ziolo and J. Y. Ying, *Nanostruct. Mater.*, 1997, **9**, 185.
11 D. Niznansky, J. L. Rehspringer and M. Drillon, *IEEE Trans. Magn.*, 1994, **30**, 821.
12 E. Tronc, P. Prene, J. P. Jolivet, F. D'Orazio, F. Lucari, D. Fiorani, M. Godinho, R. Cherkaoui, M. Nogues and J. L. Dorman, *Hyperfine Interact.*, 1995, **95**, 129.
13 F. Del Monte, M. P. Morales, D. Levy, A. Fernandez, M. Ocana, A. Roig, E. Molins, K. O'Grady and C. J. Serna, *Langmuir*, 1997, **13**, 3627.
14 C. Cannas, D. Gatteschi, A. Musinu, G. Piccaluga and C. Sangregorio, *J. Phys. Chem. B*, 1998, **102**(40), 7721.
15 G. Concas, G. Ennas, D. Gatteschi, A. Musinu, G. Piccaluga, C. Sangregorio, G. Spano, J. L. Stanger and D. Zedda, *Chem. Mater.*, 1998, **10**, 2495.
16 C. Cannas, G. Concas, A. Falqui, D. Gatteschi, A. Musinu, G. Piccaluga, C. Sangregorio and G. Spano, *Phys. Chem. Chem. Phys.*, 2001, **3**, 832.
17 C. Chaneac, E. Tronc and J. P. Jolivet, *Mater. Res. Soc. Symp. Proc.*, 2001, **628**, CC6.4.1–CC6.4.6.
18 A. Bourlinos, A. Simopoulos, D. Petridis, H. Okumura and G. Hadjipanayis, *Adv. Mater. (Weinheim, Ger.)*, 2001, **13**(4), 289.
19 C. Chaneac, E. Tronc and J. P. Jolivet, *J. Mater. Chem.*, 1996, **6**(12), 1905.
20 P. Ayyub, M. Multani, M. Barma, V. R. Polkar and R. Vijayaraghavan, *J. Phys. C: Solid State Phys.*, 1988, **21**, 2229.
21 C. Cannas, G. Concas, A. Falqui, A. Musinu, G. Piccaluga and G. Spano, *J. Non Cryst. Solids*, 2001, **286**, 64.
22 R. M. Schwertmann, and U. Cornell, *The Iron Oxides*, Weinheim, New York, 1996.
23 C. Cannas, M. F. Casula, G. Concas, A. Corrias, D. Gatteschi, A. Falqui, A. Musinu, C. Sangregorio and G. Spano, *J. Mater. Chem.*, 2001, **11**, 3180.
24 S. Mørup, H. Topsoe and J. Lipka, *J. Phys.*, 1976, **35**, C6–207.
25 L. Néel, *Ann. Geophys.*, 1949, **5**, 99.
26 S. Mørup, F. Bodker, P. V. Hendriksen and S. Linderoth, *Phys. Rev. B*, 1995, **52**, 287.
27 E. Murad and J. H. Johnston, in *Mössbauer Spectroscopy Applied to Inorganic Chemistry*, ed. G. J. Long, Plenum Press, New York, 1987, vol. 2, p. 507.
28 A. H. Morrish, *The Physical Principles of Magnetism*, Wiley, New York, 1965.
29 G. Howorth and K. Kawazoe, *J. Chem. Eng. Jpn.*, 1983, **16**, 470.
30 N. Nakamura, R. Takahashi, S. Sato, T. Sodesawa and S. Yoshida, *Phys. Chem. Chem. Phys.*, 2000, **2**, 4984.